Dalton Transactions

ROYAL SOCIETY OF CHEMISTRY

PAPER

View Article Online
View Journal | View Issue

Check for updates

Cite this: *Dalton Trans.*, 2023, **52**, 13528

Energetics of key Au(III)-substrate adducts relevant to catalytic hydroarylation of alkynes†

Matthieu Regnacq,[a] Denis Lesage,[a] Marte S. M. Holmsen,[c,d,e] Karinne Miqueu,[b] Didier Bourissou *[c] and Yves Gimbert*[a,f]

Received 26th July 2023,
Accepted 30th August 2023

DOI: 10.1039/d3dt02393a

rsc.li/dalton

(P,C)-cyclometalated Au(III) complexes have shown remarkable ability to catalyze the intermolecular hydroarylation of alkynes. Evidence of an outer-sphere mechanism has been provided in a previous study and is confirmed here by analysing the experimental data and DFT calculations. In this work, we propose evaluation of critical energies of dissociation of Au(III) complexes with different substrates *via* energy-resolved mass spectrometry (ERMS) experiments and kinetic modelling. The kinetic model is based on a multi-collisional approach. On the one hand, the classification confirms the mechanism previously proposed; on the other hand, it supports the collisional model and its application to particularly fragile adducts.

Introduction

Gold(III) catalysis has grown spectacularly during the last few years. Cyclometalated Au(III) complexes were found to catalyse novel reactions or to improve the yields and selectivity of others.[1,2] These systems are very promising, but the mechanisms of Au(III)-catalysed transformations are not well known yet. Most of the work proposing mechanisms to rationalize observed reactivities use theoretical chemistry sometimes associated with experimental explorations involving isotope labelling and/or NMR and X-ray crystallography.[2] In the difficult task of elucidating and characterizing the key intermediates in these reactions, studies of teams contributing to the understanding of gold(III) chemistry must be highlighted. In this way, Fiksdahl *et al.* recently reported a systematic study of the reactivity of Au(III) bis(pyridine) complexes used in a propargyl ester cyclopropanation reaction based on NMR and crystallographic data, combined with DFT.[3] Using the same joint approach, this team also investigated the mechanism of 1,6-enyne alkoxycyclization involving Au(III) bidentate complexes.[4] Still in the context of cyclization reactions, Hashmi *et al.* recently presented a study on the differences in reactivities observed with Pt(II) and Au(III) carbenes in the annulation of benzofurazans and ynamides.[5] Labelling experiments combined with a DFT description enabled them to highlight the importance of the cationic character of the M–carbene species, which is more pronounced in the case of Au than Pt and is at the origin of the different types of cyclization observed (by O for Au and by N for Pt). Several teams have investigated the coordination mode of alkenes and alkynes on Au(III) complexes. Bochmann *et al.*[6,7] sought to understand the influence of metal-bearing ligands on this coordination. A DFT study of M–alkyne bond lengths and the determination of binding energies enabled them to assess the importance of the *trans*-effect of ligands already present in the complex. Tilset *et al.*[8] were able to show by labelling experiments combined with DFT that in the acetylene trifluoroacetoxylation reaction, the catalytically active form of Au(III) ligated by 2-(*p*-tolyl)pyridine was not the initial complex $LAu(OAc^F)_2$ (OAc^F = $OCOCF_3$) itself but a more advanced vinyl gold intermediate $AuL(OAc^F)(CH{=}CHOAc^F)$. The activation of alkynes by Au(III) complexes has also been studied theoretically in depth by Belanzoni *et al.*[9] using charge-displacement analysis and also during the hydration of alkynes.[10,11] Studies have also been carried out on Au(III)–CO carbonyl gold complexes, species with low stability of which only a few examples have been isolated with specially adapted ligands. Bochmann *et al.* reported the first synthesis of an Au(III)–CO complex, which showed high reactivity to

[a]*Institut Parisien de Chimie Moléculaire – IPCM UMR 8232, CNRS/Sorbonne Université, 75252 Paris Cedex 05, France.*
E-mail: yves.gimbert@univ-grenoble-alpes.fr
[b]*CNRS/Université de Pau et des Pays de l'Adour, E2S-UPPA, Institut des Sciences Analytiques et de Physico-Chimie pour l'Environnement et les Matériaux – IPREM UMR 5254, 64053 Pau Cedex 09, France*
[c]*Laboratoire Hétérochimie Fondamentale et Appliquée – LHFA UMR 5069, CNRS/Université de Toulouse, UPS, 31062 Toulouse Cedex 09, France.*
E-mail: didier.bourissou@univ-tlse3.fr
[d]*Centre for Materials Science and Nanotechnology, University of Oslo, P.O. Box 1126 Blindern, N-0316 Oslo, Norway*
[e]*Department of Chemistry, University of Oslo, P.O. Box 1033 Blindern, N-0315 Oslo, Norway*
[f]*Département de Chimie Moléculaire – DCM UMR 5250, CNRS/Université Grenoble Alpes, UGA, 38000 Grenoble, France*

†Electronic supplementary information (ESI) available. See DOI: https://doi.org/10.1039/d3dt02393a

nucleophilic attack.[12] Belanzoni *et al.*[13] then used the same complex to describe the nature of the Au(III)–CO bond (again using the charge displacement method) and concluded that the Au(III)–CO coordination consists of a strong bond through σ-donation from CO to the gold center and an even stronger bond through π-backdonation from the gold center to CO; this rationalizes the behavior under nucleophilic attack of such complexes. These Au(III)–CO complexes have also been the subject of mechanistic studies by DFT involving nucleophilic attack of water, causing the extraction of CO_2 combined with a reductive C,H bond formation.[14] Recently, (P,C)-cyclometalated Au(III) complexes have shown remarkable efficiency in the intermolecular, stereoselective and atom-economical hydroarylation of alkynes.[15] Hydroarylation may be defined as the addition of an aryl group and a hydrogen atom across an unsaturated moiety, here an alkyne, that yields a new Csp^2–Csp^2 bond (Scheme 1). Such a reaction is very advantageous compared to classical cross-coupling processes, in which formal hydroarylation products are derived from pre-functionalized aromatic substrates. It has been shown by Bourissou and coworkers that the reaction proceeds by an outer-sphere mechanism,[16] involving the nucleophilic addition of an electron-rich arene to the π-coordinated alkyne in gold. The first evidence in favour of this mechanism was the *anti*-addition of the arene to the C≡C triple bond. This study was supported by NMR and mass spectrometry experiments, and by DFT calculations. Mass spectrometry is a powerful tool for detecting reactive ionic intermediates and sometimes even for decrypting full reaction mechanisms.[17–19]

Au(III) complexes are usually tetracoordinated and adopt square planar geometry. The removal of one OAc^F from [(P,C)$Au(OAc^F)_2$] is an endothermic reaction. It is favoured in the presence of $B(C_6F_5)$ (liquid phase) or by increasing the cone voltage (gas phase). Mass spectrometry, DFT calculations and low-temperature NMR spectroscopy experiments showed that the active species holds one trifluoroacetate group OAc^F and suggested that it is κ^2-coordinated. This κ^2 form is both stable enough to prevent the catalyst from degradation and reactive enough to allow catalysis. This type of species, well-balanced between stability and reactivity, is highly suited for synthetic processes. The transformation of the κ^2 form to the three-coordinate κ^1 form allows the introduction of a substrate into the coordination sphere of Au(III). It has been shown that both diphenylacetylene (DPA) and 1,3,5-trimethoxybenzene (1,3,5-TMB) can bind to the Au(III) center. According to MS and DFT, the 1,3,5-TMB adduct is energetically favoured compared with the diphenylacetylene (DPA) adduct. This is consistent with the stable σ-arene intermediate (Wheland intermediate), identified as a resting state, which was isolated and characterized by NMR spectroscopy. In the gas phase, the ternary adduct $[(P,C)Au(OAc^F)(TMB)(DPA)]^+$ has been observed. The loss of DPA is not observed in the fragmentation spectrum of the ternary adduct, suggesting that the alkyne is in the first coordination sphere, while the arene enters the second one.

As a consequence, the outer-sphere reaction of hydroarylation involves a subtle balance between the stability of the gold–arene adduct and the necessity to activate the C≡C triple bond (DPA needs to be in the first coordination sphere of gold). In this work, the objective was to compare, at least qualitatively, the bond dissociation energies of adducts between the $[(P,C)Au^{III}(OAc^F)]^+$ active species and different alkynes and arenes. It is of primary interest to determine how much the Wheland intermediate (resting state) is stabilized compared to the activated alkyne complex and the ease of carrying out catalytic hydroarylation.

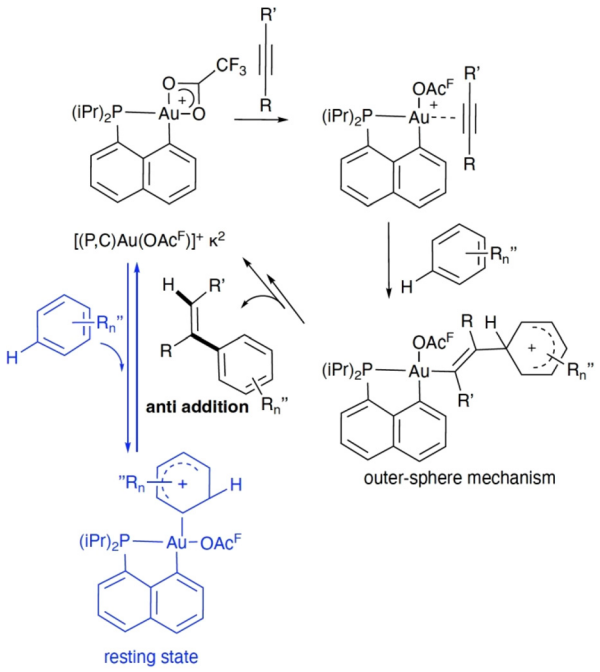

Scheme 1 Mechanism of the hydroarylation of alkynes catalyzed by (P,C)$Au(OAc^F)$.

Materials and methods

Mass spectrometry

The (P,C)-cyclometalated precatalyst [(P,C)$Au(OAc^F)_2$] was synthesized according to a previously published procedure[15] and was infused with 1×10^{-4} M substrate in acetonitrile at 15 μL min^{-1}. The substrates that have been used for this study are presented in Fig. 1. The experiments were performed on a home-modified triple quadrupole mass spectrometer (Quattro II, Waters) equipped with an electrospray (ESI) source.[20] In Fig. 2, the different distances that account for the kinetic modelling are presented. The temperature of the source was fixed at 100 °C. The signal corresponding to the $[(P,C)Au(OAc^F)]^+$ ion significantly increased when a minimum cone voltage of 50 V was applied. The substrates were introduced into the transfer hexapole (H0) *via* tubing lines under vacuum. Some of them were not volatile enough to be introduced directly into the mass spectrometer under vacuum conditions. Thus, a heated line was installed in order to allow the introduction of less-volatile substrates into the transfer hexapole preceding the

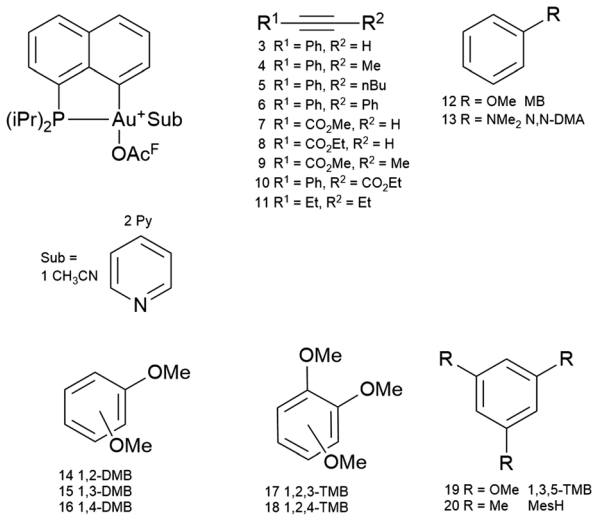

Fig. 1 Catalyst and substrates considered in this study. MB, DMB, and TMB stand for methoxybenzene, di-methoxybenzene, and tri-methoxybenzene, while DMA denotes dimethylamine, and MesH is mesitylene. The numbers designate the corresponding binary complexes.

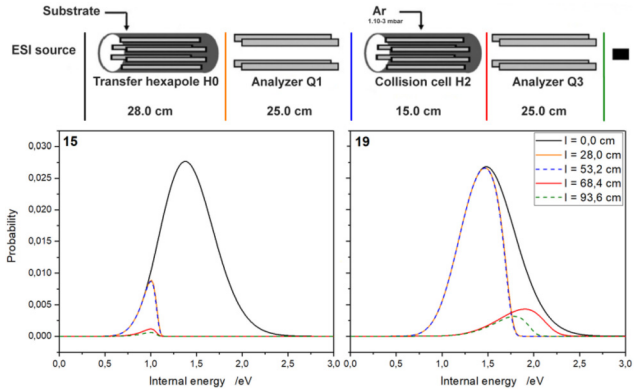

Fig. 2 General scheme of the ESI-triple quadrupole used in this study (top). Simulated internal energy distributions of complex **15** [(P,C)Au(OAc^F)(1,3-DMB)]$^+$ (E_0 16.5 kcal mol^{-1}) and complex **19** [(P,C)Au(OAc^F)(1,3,5-TMB)]$^+$ (E_0 21.8 kcal mol^{-1}), at different places of the instrument (bottom). The pressure of Ar was set to 1 × 10^{-3} mbar and V_{coll} (accelerating voltage) was set to 10 V.

first quadrupole.[16] The strategy involves forming the adducts in the gas phase by ion–molecule reactions in the hexapole that precedes the first quadrupole, before colliding them with gas in the collision cell while increasing the collision energy. A Pirani gauge was used to measure the pressure in the collision cell. The determination of bond dissociation energies (as seen in many examples in the literature, even with gold complexes[21]) is based on the principle of energy-resolved mass spectrometry (ERMS) experiments. The size effect was taken into account by converting the kinetic energy of the precursor ion, E_{lab}, into center-of-mass energy, E_{COM}, using $E_{COM} = \mu \cdot E_{lab}$, where μ is $M_{gas}/(M_{gas} + M_{ion})$. The survival yield (SY) is defined as the intensity of the precursor ion divided by the sum of the intensities of the precursor ion and all its fragment ions. The fragment yield (FY) is defined as the intensity of the main fragment ion divided by the sum of the intensities of the precursor ion and all its fragment ions.

Molecular modelling

Geometry optimizations and frequency calculations were carried out using Gaussian16[22] at the B97D/SDD+f(Au),6-31G** (other atoms) level of theory in the gas phase for each complex. DLPNO-CCSD(T) calculations were carried out using ORCA 5.0[23] based on the optimized geometries obtained with DFT. The cc-PVTZ basis set was used for all atoms except for gold where cc-PCTZ-PP was employed. The SK-MCDHF-RSC electron-core potential was added for gold. When several isomers exist on the potential energy surface (PES), only the most stable have been considered. The following equation was used to determine the bond dissociation energy:

$$\mathrm{BDE} = \left(E_{\mathrm{CCSD(T)}} + \mathrm{ZPE_{DFT}}\right)_{\mathrm{Au\text{-}\kappa^2}} + \left(E_{\mathrm{CCSD(T)}} + \mathrm{ZPE_{DFT}}\right)_{\mathrm{Sub}} - \left(E_{\mathrm{CCSD(T)}} + \mathrm{ZPE_{DFT}}\right)_{\mathrm{Adduct}} + \mathrm{BSSE_{CCSD(T)}}$$

where Au-κ^2, Sub and Adduct designate the [(P,C)Au(OAc^F)]$^+$ κ^2 precursor ion, the substrate, and the [(P,C)Au(OAc^F)(substrate)]$^+$ adduct, respectively. ZPE is the zero-point energy correction, calculated at the DFT level of theory, and BSSE is the basis set superposition error, calculated at the CCSD(T) level of theory.

Kinetic modelling

MassKinetics[24] (Version 2.1.2.696) was used to fit the experimental SY and FY curves. The critical dissociation energies E_0 of these gold complexes were determined. A loose transition state was defined by reducing the five lower frequencies[25,26] to obtain a logarithm of the pre-exponential factor equal to 17. The temperature of the ions was set to the temperature of the source (373 K). The efficiency of collisions was set to 0.25, which is in the interval of recommended values.[24] The energy transfer function proposed by F. Muntean and P.B. Armentrout[27] was used. Uncertainties are mainly based on the collision gas pressure (±1 × 10^{-4} mbar), the temperature (±10 K), the logarithm of the pre-exponential factor (±1.0), the efficiency of the collision (±0.05) and the collision cross-section, CCS (±10.0 Å^2). The CCS was estimated, thanks to IMoS 1.10 software[28] and the TMLJ method. Default Lennard–Jones parameters were used. Argon (or xenon) was set as the gas and the temperature of the gas was set at 298 K. In order to check if the model is acceptable, a 5 × 10^{-5} M gold complex solution in excess B(C$_6$F$_5$)$_3$ was injected into a TIMS-TOF instrument (Bruker). A difference of 3% was observed between the experimental and calculated values for the precursor [(P,C)Au(OAc^F)]$^+$ ion.

Results and discussion

Binary adducts

Internal energy distributions have been simulated with MassKinetics at different points of the triple quadrupole

instrument (ESI source: 0.0 cm, end of H0: 28.0 cm, end of Q1: 53.2 cm, end of collision cell H2: 68.4 cm, end of Q3: 93.6 cm) and are presented for two complexes, **15** and **19** (Fig. 2). According to their calculated BDE, **19** is more difficult to break than **15** (see Table 1, most stable isomers). These figures, especially the one for **15**, show that the complexes are partially broken a few centimeters (so, a dozen microseconds) after their formation in the first hexapole. This can be related to thermal decomposition or to fragmentation caused by collisions, since there is residual N_2 gas from the ESI source. The internal energy distribution curves appear as truncated distributions. Simulations have shown that only a few centimeters of flight are efficient enough to obtain these truncated internal energy distributions. Thus, in the case of weak adducts, like **15** $[(P,C)Au(OAc^F)(1,3\text{-DMB})]^+$, only ~10% of the ions pass through hexapole H0. We note that all adducts that have a BDE below 15 kcal mol^{-1} do not yield exploitable SY curves (no signal, wide variations of the signal and/or of the SY curve, or impossibility to fit the curves in an acceptable way). The complexes are so fragile that they are mostly fragmented in the H0-Q1 sequence. Mainly background noise is isolated with the first quadrupole. Thus, complexes **7**, **8**, **9**, **12**, **16** and **20** have not been treated. The internal energy of the ions before/after the MSMS step is indicated in red/green in Fig. 2. They correspond to collisional excitation and fragmentation in H2. The complexes were formed by ion–molecule reactions in the hexapole preceding the first quadrupole. Different alkynes and arenes were tested (Fig. 1). Their electron-rich π systems grant them a particular affinity for high-valent Au(III), as observed in the condensed phase.

Indeed, some Au(III)-π complexes have already been characterized.[29] Also, arenes are expected to form Wheland complexes before possible proton transfer.[16,30] First, we studied the simple gold(III) alkyne or arene adducts, and tried to determine their critical energies of dissociation. Then, we investigated the formation and fragmentation of ternary adducts $[(P,C)Au(OAc^F)(alkyne)(arene)]^+$. In Fig. 3, the experimental SY plots and their associated simulated curves are plotted. The curves were fitted in search of the best compromise with the SY axis set at normal and logarithmic scale (Fig. S4†). Note that at low collision voltages, the measured experimental SY is sometimes far from the calculated SY. This is due to two reasons. First, the gas pressure prevents certain ions from reaching the detector. The ions are, so to say, stopped in the collision cell and not transmitted. On the other hand, the kinetic energy distribution around the collision energy value is relatively wide.[31] The E_0 parameters used to fit the SY plots are reported in Table 1. It appears clearly that complex **2** (with pyridine) is the strongest complex, followed far behind by **19**, **13** and **3**. The critical energy of dissociation of complex **3** $[(P,C)Au(OAc^F)(PhCCH)]^+$ is not in accordance with the BDE calculation result. This outlier is discussed separately below. Then come the other trimethoxybenzene complexes, **17** and **18** (due to the electron density brought by the methoxy groups). Adducts **5**, **10** and **11** can also be considered moderately strong. Complexes **4**, **6**, **14** and **15** are the most fragile that can be treated.

Comparison of our model with the TCID technique

The threshold CID (TCID) technique is one of the gold-standards for the determination of bond dissociation energies (BDE),[32–36] as well as the BIRD technique.[37] We have estimated the critical energy of dissociation (E_0) for some complexes (complexes **4** and **19**, as shown in Fig. 4; **2** and **6**, as shown in Fig. S5†) by TCID. For each complex, the estimated E_0 was found to be close to the calculated BDE. However, the complexes considered here are so fragile (except **2**) that the slightest collision energy is enough to break up large parts of the

Table 1 Experimental critical energies (E_0 in kcal mol^{-1}) and bond dissociation energies (BDE_{calc} in kcal mol^{-1}) calculated at the DLPNO-CCSD(T) level of theory. Gold–substrate (Au–Sub) distances are given in Å. Isomers with substrates *trans* to the P atom have been found to be more stable. When different isomers have been optimized (O *vs.* C or C≡C adduct), the different binding modes are also indicated. Diverse meaningful structures have been tested: only the most stable isomer of each kind is presented

	Substrate	Distance Au–Sub	BDE_{calc}	E_0		Substrate	Distance Au–Sub	BDE_{calc}	E_0
1	CH_3CN	Au–N 2.17	17.4	16.7 ± 3.3	**11**	EtCCEt	Au–(CC) 2.40	19.0	18.7 ± 2.6
2	Py	Au–N 2.17	31.0	30.0 ± 2.5	**12**	MB (anisole)	Au–C 2.44	14.5	—
							Au–O 2.26	10.3	
3	PhCCH	Au–(CC) 2.27	13.0	**21.9 ± 2.5**	**13**	*N*,*N*-DMA	Au–N 2.33	21.5	20.8 ± 2.3
							Au–C 2.38	19.5	
4	PhCCMe	Au–(CC) 2.33	18.3	16.6 ± 3.3	**14**	1,2-DMB	Au–O 2.37	17.6	15.5 ± 3.3
							Au–C 2.40	12.6	
5	PhCCnBu	Au–(CC) 2.30	20.5	18.7 ± 2.6	**15**	1,3-DMB	Au–C 2.33	16.5	16.1 ± 3.4
							Au–O 2.25	12.5	
6	PhCCPh	Au–(CC) 2.37	19.4	17.3 ± 2.9	**16**	1,4-DMB	Au–O 2.25	13.9	—
							Au–C 2.43	11.7	
7	$HCCCO_2Me$	Au–O 2.21	9.5	—	**17**	1,2,3-TMB	Au–O 2.24	19.5	18.9 ± 3.1
		Au–(CC) 2.44	5.2				Au–C 2.35	16.2	
8	$HCCCO_2Et$	Au–O 2.21	11.1	—	**18**	1,2,4-TMB	Au–C 2.34	18.5	18.4 ± 2.7
		Au–(CC) 2.44	6.2				Au–O 2.36	16.0	
9	$MeCCCO_2Me$	Au–O 2.20	12.8	—	**19**	1,3,5-TMB	Au–C 2.29	21.8	21.7 ± 2.3
		Au–(CC) 2.35	11.0				Au–O 2.27	11.6	
10	$PhCCCO_2Et$	Au–O 2.17	19.6	18.9 ± 2.7	**20**	MesH	Au–C 2.39	12.7	—
		Au–(CC) 2.23	14.4						

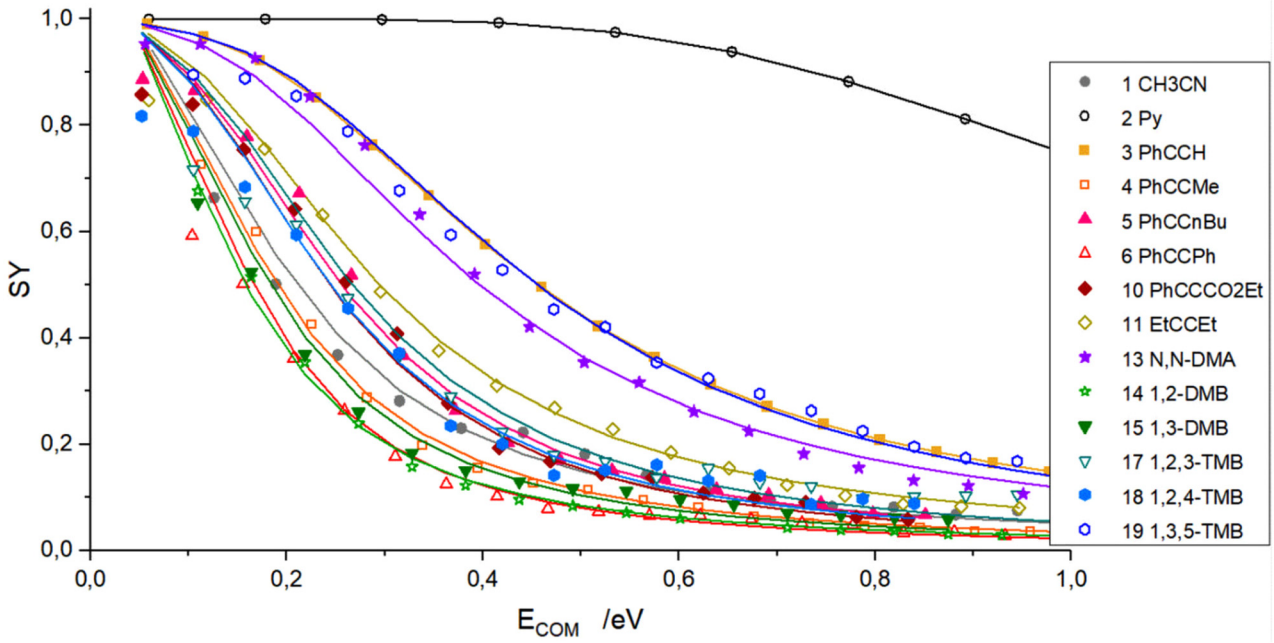

Fig. 3 Fragmentation curves of the different adducts. Plots and curves are reported according to the E_{COM} scale. Experimental data points and calculated fits are presented on a linear SY scale.

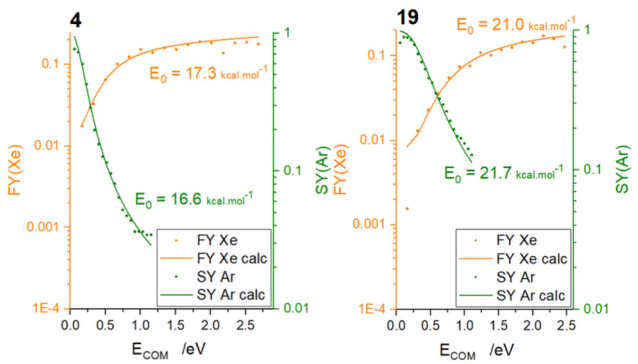

Fig. 4 Comparison of TCID (orange) and CID (green) experiments for complexes **4** $[(P,C)Au(OAc^F)(PhCCMe)]^+$ and **19** $[(P,C)Au(OAc^F)(1,3,5\text{-}TMB)]^+$. TCID conditions: 6×10^{-5} mbar of Xe in the collision cell. CID conditions: 1×10^{-3} mbar of Ar in the collision cell.

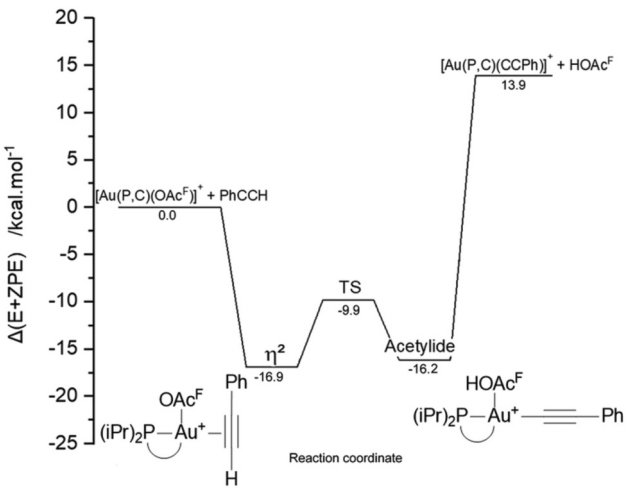

Fig. 5 Energy profile for the formation of acetylide in the particular case of phenylacetylene. Energies ($\Delta(E + ZPE)$ in kcal mol^{-1}) are calculated with CCSD(T) (uncorrected for BSSE), on the geometries optimized at the B97D/SDD+f (Au),6-31G(d,p) (other atoms) level of theory.

ions (see below). Thus, the threshold measure becomes unclear because the dynamic range of fragmentation is too narrow. This is why we chose to work under multiple-collision conditions. The argon pressure was set to 1×10^{-3} mbar in the collision cell. Relatively good agreement was found between the TCID and CID experiments.

Special case of the PhCCH adduct

According to its low BDE, the critical energy of dissociation of the phenylacetylene adduct **3** should be much lower. In contrast, it appears to be almost as strong as that for **19** (Fig. 3). The acetylenic proton of PhCCH is acidic and it is highly likely that the corresponding acetylide species is involved in the dissociation process, as supported by the appearance of a minor peak corresponding to the loss of $HOAc^F$ (−114 Da, or −115 Da when PhCCD is used). The existence of such species has already been established for Au(I)[38] as well as Pd(II) and Pt (II).[39] The acetylide structure was calculated to be 0.7 kcal mol^{-1} slightly less stable than the η^2 form (Fig. 5; the energy values presented here are CCSD(T) values). The transition state (TS) connecting the η^2 and acetylide forms (proton transfer from the terminal carbon atom to the OAc^F group) is only

7.0 kcal mol^{-1} higher in energy, and is thus easily obtained. Concerning kinetic modelling, the MassKinetics model used in this study does not take into account well the equilibrium between the η^2 and acetylide forms. Therefore, we have developed a new model, which is described in the ESI.† This model is no longer based on collisions but on thermal activation (due to the multi-collisional regime), by attributing a temperature value to a collision voltage. This model better takes into account the equilibrium between the η^2 and acetylide forms and gives a reliable E_0 value (14.1 kcal mol^{-1}) for the dissociation of PhCCH from $[(P,C)Au(OAc^F)(PhCCH)]^+$, which is close to the calculated one. The model has been tested successfully on other complexes (Fig. S3†).

Correlation between experiments and theory

Fig. 6 is a plot of the experimental critical energies E_0 extracted from the SY curves by kinetic modelling against the calculated bond dissociation energies. At values below E_0 = 15 kcal mol^{-1}, no experimental data points were obtained, except in the particular case of PhCCH. This "no point's zone" is a consequence of the fragmentation in the transfer hexapole or in the first quadrupole of the most fragile adducts.

In some cases (**10**, **13**, **14**, **15**, **17**, **18**, and **19** are concerned), different coordination types can be envisioned (Fig. 7). They cannot be distinguished on the basis of the MS/MS spectrum (same fragments), but critical energy values may enable doing so. In the source, there is an equilibrium between the different isomers that favors the most stable one. However, the most fragile isomers are more likely to easily transition towards the ground-state structure or to fragment in the transfer hexapole. It is clear then that the most stable conformer is present at much higher yields in the collision cell.

The set of E_0 values determined experimentally by MS matches well with the BDE values computed by DLPNO-CCSD

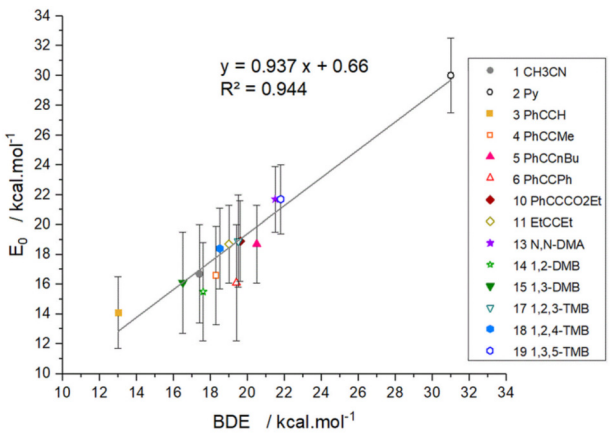

Fig. 6 E_0 *vs.* BDE (in kcal mol^{-1}) plot. The error bars indicated on the graph are not uncertainties calculated from experimental variations, but biases established in the kinetic model. They include the bias on the pre-exponential factor (17.0 ± 1.0), on the pressure in the collision cell (1 × 10^{-3} ± 1 × 10^{-4} mbar), the temperature of the source (373 ± 10 K), the collision cross-section (±10 Å^2) and the coefficient of inelasticity (0.25 ± 0.05).

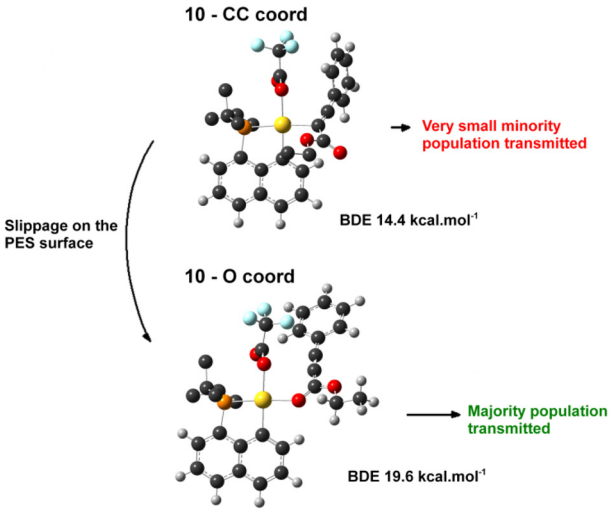

Fig. 7 Optimized structures of complex **10** involving O and C≡C coordinations. Some H atoms were removed for the sake of clarity. Au: yellow, P: orange, C: black, F: light blue, O: red, and H: grey.

(T) calculations. For most of the complexes, the computed BDE value falls within the margin of error of the E_0 determination value determined experimentally upon kinetic modelling. The slope of the linear regression and the intercept are 0.94 and 0.66, respectively, which are close to the ideal coefficients of 1 and 0. A pretty good agreement is found between E_0 and BDE (R^2 = 0.944). These three parameters are the indicators of good correlation between E_0 and BDE. Based on the consistency of the calculations, we can assert that the kinetic model used in this study is well adapted to these kinds of fragile compounds. Nonetheless, there are some limitations in the use of this model. First of all, the signal used to calculate the SY needs to be high enough. The pre-exponential factor was also considered to be 17.0 (reflecting a loose TS), which is just a primary approximation justified by the fact that no TS associated with the decoordination of the substrate was found on the PES, suggesting that the process is barrierless.

Within the series of methoxy-substituted benzenes, the greater the number of methoxy groups, the higher the critical energy of dissociation, the smaller the Au–C distance and the higher the electronic density on the aromatic ring, especially at the *ortho* and *para* positions (NPA charges on arenes are presented in Fig. S1†). Calculated bond dissociation energies support this observation. It is obvious that the CH(arene) positions of 1,3,5-TMB are particularly electron rich because they are all at *ortho*- and *para*-positions of the OMe groups, in contrast to 1,2,3-TMB and 1,2,4-TMB in which unfavorable *meta* positions also exist.

Within the series of alkynes, the BDEs and critical energies of **4**, **5**, **6**, **10** and **11** are so close that it appears more difficult to reveal a general trend. The strength of alkyne coordination most likely depends on several factors, *i.e.*, the electron density and polarization of the CC triple bond, as well as the steric hindrance induced by substituents.

The case of CO_2R-substituted alkynes also deserves comments. The ester group lowers the electron density of the C≡C triple bond to such an extent that O coordination is favored, also underlying the oxophilic character of Au(III)[40,41] (Fig. 7). In the gas phase, no ternary adducts were detected when PhC≡CCO_2Et was used as the alkyne and 1,3,5-TMB as arene: only the binary adducts **10** and **19** were observed. An explanation can be offered by considering the differences in BDE observed for **10** (Table 1, entry 10), which indicates that in the gas phase, alkyne coordination takes place preferentially *via* O (19.6 *vs.* 14.4 kcal mol^{-1} for coordination *via* the C≡C bond). This coordination *via* the O atom seems to be specific to the gas phase (which induces kinetic control), because in solution, the use of PhCCCO_2Et leads to the reaction product.[15]

Ternary adducts and protodeauration process

We generated several ternary adducts in the gas phase, by introducing both the alkyne and the arene at the same time into the first hexapole. When the two substrates are not very volatile, they were both introduced through the heated line. The line temperature was set to a temperature for which we can systematically ensure the presence of the binary adducts with the alkyne and with the arene, before looking for the presence of the ternary adduct. In the gas phase, only ternary adducts with 1,3,5-TMB as the arene have been observed, although in solution, hydroarylation was also done with other arenes.[15] Therefore, only 1,3,5-TMB as an arene seems to be nucleophilic enough to react with activated π-alkyne complexes in the gas phase. This underlines once again the electron-rich and activated nature of 1,3,5-TMB as substrate. The alkynes used are PhCCH, PhCCMe, PhCCnBu, PhCCPh, PhCCCO_2Et and EtCCEt. Noticeably, all attempts to form and characterize the ternary adduct [(P,C)Au(OAc^F)(PhCCCO_2Et)(1,3,5-TMB)]$^+$ remained unsuccessful.

CID-MS/MS spectra of the ternary adducts have been recorded (Fig. S6†). The fragmentation spectrum of [(P,C)Au(OAc^F)(PhCCPh)(1,3,5-TMB)]$^+$ (*m*/*z* 899) shows *m*/*z* 731 [(P,C)Au(OAc^F) (PhCCPh)]$^+$ and *m*/*z* 553 [(P,C)Au(OAc^F)]$^+$ (see the ESI†), which may correspond to the loss of the hydroarylation product (styrene derivative) or to the concomitant (and consecutive) losses of 1,3,5-TMB and PhCCPh, in this order. The loss of PhCCPh from *m*/*z* 899 is not observed, which is additional evidence for the outer-sphere mechanism. All the MS/MS spectra are similar to the spectrum obtained with PhCCPh as the alkyne. The CID-MS/MS spectrum of *m*/*z* 803 (ternary adduct [(P,C)Au(OAc^F)(EtCCEt)(1,3,5-TMB)]$^+$) does not show the loss of 1,3,5-TMB (168 Da) or EtCCEt (82 Da) but does show the loss of 250 Da (168 + 82 Da), corresponding to the loss of the hydroarylation product and/or the concomitant losses of 1,3,5-TMB and the alkyne. Unfortunately, we were not able to record fragmentation curves of [(P,C)Au(OAc^F)(alkyne)(1,3,5-TMB)]$^+$ ions due to the low intensity of the corresponding peaks.

Fig. 8 shows the full hydroarylation pathway computed in the gas phase for the reaction between reactants PhCCPh and 1,3,5-TMB promoted by the [(P,C)Au(OAc^F)]$^+$ complex. The

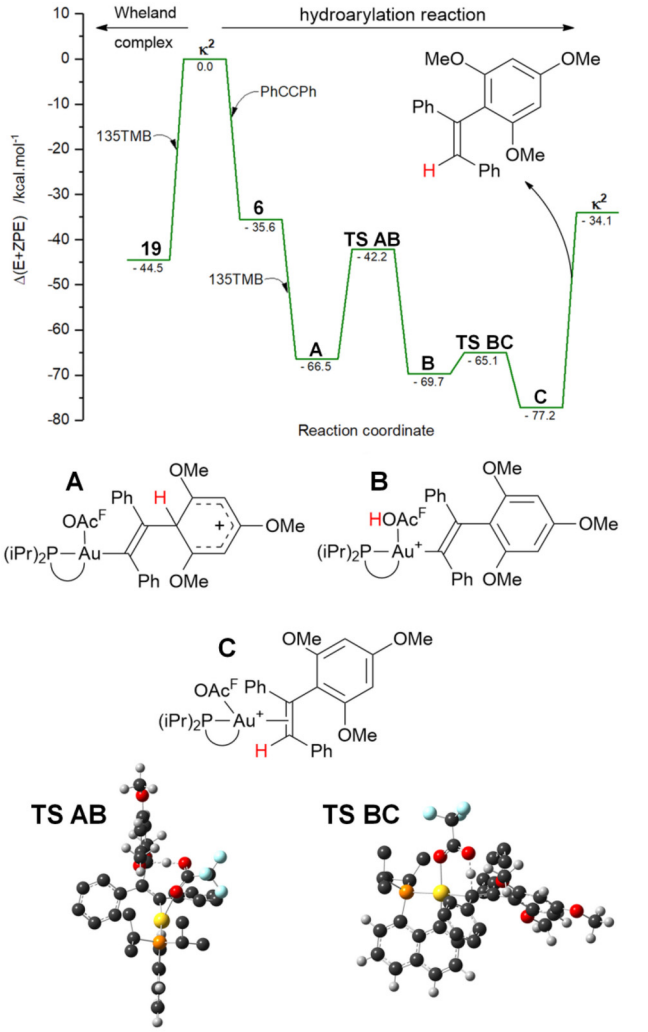

Fig. 8 Full outer-sphere mechanism computed in the gas phase for the hydroarylation between PhCCPh and 1,3,5-TMB promoted by the [(P,C)Au(OAc^F)]$^+$ complex (R = iPr) and OAc^F *cis* to P. The *E* + ZPE energies have been calculated at the B97D/SDD+f (Au),6−31G(d,p) (other atoms) level of theory, in the gas phase. Some H atoms were removed for the sake of clarity on TS structures. Au: yellow, P: orange, C: black, F: light blue, O: red, and H: grey.

hydroarylation mechanism is composed of two main steps: the formation of the C–C bond ([κ^2-(P,C)Au(OAc^F)]$^+$ → intermediate **A**), followed by protodeauration (**A** to **C**). The PhCCPh coordination is not competitive energetically with that of 1,3,5-TMB (−35.6 kcal mol^{-1} against −44.5 kcal mol^{-1}), in line with our experimental observations. However, the nucleophilic addition of 1,3,5-TMB to the π-activated alkyne complex is very much favored energetically (−66.5 kcal mol^{-1}) and is a barrierless process (no TS localized on PES in the gas phase). The deprotonation of 1,3,5-TMB by the OAc^F group followed by the protodeauration step (migration of the proton from $HOAc^F$ to the styrene product) is not too energetically demanding. The protodeauration might be seen as the replacement of Au(III) by a proton (that comes from the arene moiety), to allow the

decoordination of the hydroarylation product. The proton transfer from the arene moiety to OAc^F requires 24.3 kcal mol^{-1} (**A** → **TS AB**) in the gas phase. This energy barrier is lower than the one needed to decoordinate 1,3,5-TMB (30.9 kcal mol^{-1}). Moreover, the fragment peak corresponding to the loss of the styrene derivative (m/z 553) is always more intense than that corresponding to the loss of 1,3,5-TMB. The last step of the mechanism is the back migration of the proton from HOAcF to the carbon atom (**B** → **C**). This step needs only a little bit of energy to be completed (**B** → **TS BC**, 4.6 kcal mol^{-1}). The ensuing π-alkene complex **E** is 10.7 kcal mol^{-1} lower in energy than the ternary adduct **A**. Similar profiles were computed for the reaction of 1,3,5-TMB with the other alkynes (the energies of the key intermediates and transition states are collected in Table S1†).

Conclusions

To conclude, we conducted a systematic study of alkyne and arene coordination with a (P,C)-cyclometalated Au(III) complex in the context of catalytic hydroarylation of alkynes. Fragmentation curves from CID-MS/MS experiments were obtained. The kinetic modelling of these curves was carried out using MassKinetics, and critical dissociation energies E_0 were extracted from the collision model with a confidence interval of approximately 3 kcal mol^{-1}. We obtained a very good correlation between the experimental E_0 and the calculated BDE values. In turn, this suggests that the kinetic model used in this study, with collision gas at high pressure, is rather consistent, even if it is not a standard method to determine critical energies of dissociation/bond dissociation energies. It seems well adapted to relatively fragile complexes to obtain a broader dynamic range of fragmentation to fit. The experimental MS data supports the calculations previously made by Bourissou and co-workers. Indeed, the electron-rich arene 1,3,5-TMB is a better ligand towards Au(III) than any alkynes. However, outer-sphere nucleophilic addition of the arene to the π-activated alkyne is energetically favoured over the coordination of the arene alone, and the formation of the C(alkyne)–C(arene) bond stands as a sizeable driving force. We have established the full hydroarylation pathway: it is relatively easy to obtain the styrene product. Only the proton transfer from 1,3,5-TMB to OAc^F requires a little amount of energy, which is lower than the energy required to break the C–C bond between the arene and the alkyne (decoordination of 1,3,5-TMB). This study marks significant progress in different respects. First, it completes the panoply of methods for the determination of critical energies by the determination of BDEs for relatively fragile complexes. This work also permits discrimination of coordination modes in some cases (at least qualitatively) and determines absolute critical energies of dissociation. Finally, mass spectrometry once again shows that it can be used to elucidate complex molecular mechanisms and may be used for others, as long as they involve reactive ions.

Author contributions

MSMH synthesized the Au(III) complex and conducted its characterization. MR performed and analysed the MS experiments, made the kinetic model and wrote the draft. MR, KM and YG took care of molecular modelling. DL, DB, YG reviewed the paper. DB and YG designed the study.

Conflicts of interest

There are no conflicts of interest to declare.

Acknowledgements

This work was supported by GOLD(III), a grant from the Agence Nationale de la Recherche (postdoc funding of MR, ANR-19-CE07-0037). CNRS, SU, UGA and UPS are gratefully thanked for their support. This study is part of the FRINATEK project 315004 funded by the Research Council of Norway (stipend to MSMH). The computations presented in this article were performed using MESU (SU) and GRICAD (UGA) platforms and the cluster of UPPA.

References

1 R. Kumar and C. Nevado, *Angew. Chem., Int. Ed.*, 2017, **56**, 1994–2015.
2 L. Rocchigiani and M. Bochmann, *Chem. Rev.*, 2021, **121**, 8364–8451.
3 A. C. Reiersølmoen, D. Csókás, S. Øien-Ødegaard, A. Vanderkooy, A. K. Gupta, A.-C. C. Carlsson, A. Orthaber, A. Fiksdahl, I. Pápai and M. Erdélyi, *J. Am. Chem. Soc.*, 2020, **142**, 6439–6446.
4 A. C. Reiersølmoen, D. Csókás, I. Pápai, A. Fiksdahl and M. Erdélyi, *J. Am. Chem. Soc.*, 2019, **141**, 18221–18229.
5 H. Jin, W.-Y. Tong, J. Zhang, M. Rudolph, F. Rominger, X. Shen, S. Qu and A. S. K. Hashmi, *Nat. Commun.*, 2022, **13**, 1672.
6 L. Rocchigiani, J. Fernandez-Cestau, G. Agonigi, I. Chambrier, P. H. M. Budzelaar and M. Bochmann, *Angew. Chem., Int. Ed.*, 2017, **56**, 13861–13865.
7 I. Chambrier, L. Rocchigiani, D. L. Hughes, P. M. H. Budzelaar and M. Bochmann, *Chem. – Eur. J.*, 2018, **24**, 11467–11474.
8 M. S. M. Holmsen, A. Nova, D. Balcells, E. Langseth, S. Øien-Ødegaard, R. H. Heyn, M. Tilset and G. Laurenczy, *ACS Catal.*, 2017, **7**, 5023–5034.
9 L. Gregori, D. Sorbelli, L. Belpassi, F. Tarantelli and P. Belanzoni, *Inorg. Chem.*, 2019, **58**, 3115–3129.
10 J. Segato, A. Del Zotto, L. Belpassi, P. Belanzoni and D. Zuccaccia, *Catal. Sci. Technol.*, 2020, **10**, 7757–7767.
11 F. Sabatelli, J. Segato, L. Belpassi, A. Del Zotto, D. Zuccaccia and P. Belanzoni, *Molecules*, 2021, **26**, 2445.

12 D.-A. Roşca, J. Fernandez-Cestau, J. Morris, J. A. Wright and M. Bochmann, *Sci. Adv.*, 2015, **1**, e1500761.
13 C. A. Gaggioli, L. Belpassi, F. Tarantelli and P. Belanzoni, *Chem. Commun.*, 2017, **53**, 1603–1606.
14 A. Ahrens, D. M. Lustosa, L. F. P. Karger, M. Hoffmann, M. Rudolph, A. Dreuw and A. S. K. Hashmi, *Dalton Trans.*, 2021, **50**, 8752–8760.
15 C. Blons, S. Mallet-Ladeira, A. Amgoune and D. Bourissou, *Angew. Chem., Int. Ed.*, 2018, **57**, 11732–11736.
16 M. S. M. Holmsen, C. Blons, A. Amgoune, M. Regnacq, D. Lesage, E. D. Sosa Carrizo, P. Lavedan, Y. Gimbert, K. Miqueu and D. Bourissou, *J. Am. Chem. Soc.*, 2022, **144**, 22722–22733.
17 *Reactive intermediates: MS investigations in solution*, ed. L. S. Santos, Wiley-VCH, Weinheim, 2010.
18 D. Schröder, *Acc. Chem. Res.*, 2012, **45**, 1521–1532.
19 D. Lesage, A. Milet, A. Memboeuf, J. Blu, A. E. Greene, J.-C. Tabet and Y. Gimbert, *Angew. Chem., Int. Ed.*, 2014, **53**, 1939–1942.
20 D. Lesage, A. Memboeuf, Y. Gimbert and J.-C. Tabet, *Int. J. Mass Spectrom.*, 2012, **319–320**, 31–39.
21 D. Gatineau, D. Lesage, H. Clavier, H. Dossmann, C. H. Chan, A. Milet, A. Memboeuf, R. B. Cole and Y. Gimbert, *Dalton Trans.*, 2018, **47**, 15497–15505.
22 M. J. Frisch, *et al.*, *Gaussian 16, Revision C.01*, Gaussian, Inc., Wallingford CT, 2016.
23 F. Neese, *Wiley Interdiscip. Rev.: Comput. Mol. Sci.*, 2012, **2**, 73–78.
24 L. Drahos and K. Vékey, *J. Mass Spectrom.*, 2001, **36**, 237–263.
25 P. D. Schnier, W. D. Price, E. F. Strittmatter and E. R. Williams, *J. Am. Soc. Mass Spectrom.*, 1997, **8**, 771–780.
26 R. A. Jockusch and E. R. Williams, *J. Phys. Chem. A*, 1998, **102**, 4543–4550.
27 F. Muntean and P. B. Armentrout, *J. Chem. Phys.*, 2001, **115**, 1213–1228.
28 V. Shrivastav, M. Nahin, C. J. Hogan and C. Larriba-Andaluz, *J. Am. Soc. Mass Spectrom.*, 2017, **28**, 1540–1551.
29 C. Blons, A. Amgoune and D. Bourissou, *Dalton Trans.*, 2018, **47**, 10388–10393.
30 C. Boga, E. Del Vecchio, L. Forlani, A. Mazzanti, C. M. Lario, P. E. Todesco and S. Tozzi, *J. Org. Chem.*, 2009, **74**, 5568–5575.
31 D. Gatineau, A. Memboeuf, A. Milet, R. B. Cole, H. Dossmann, Y. Gimbert and D. Lesage, *Int. J. Mass Spectrom.*, 2017, **417**, 69–75.
32 M. T. Rodgers, K. M. Ervin and P. B. Armentrout, *J. Chem. Phys.*, 1997, **106**, 4499–4508.
33 P. B. Armentrout, in *Modern Mass Spectrometry*, ed. C. A. Schalley, Springer, Berlin, Heidelberg, 2003, pp. 233–262.
34 M.-E. Moret and P. Chen, *Organometallics*, 2007, **26**, 1523–1530.
35 S. Narancic, A. Bach and P. Chen, *J. Phys. Chem. A*, 2007, **111**, 7006–7013.
36 M. T. Rodgers and P. B. Armentrout, *Chem. Rev.*, 2016, **116**, 5642–5687.
37 R. C. Dunbar, *Mass Spectrom. Rev.*, 2004, **23**, 127–158.
38 A. Simonneau, F. Jaroschik, D. Lesage, M. Karanik, R. Guillot, M. Malacria, J.-C. Tabet, J.-P. Goddard, L. Fensterbank, V. Gandon and Y. Gimbert, *Chem. Sci.*, 2011, **2**, 2417–2422.
39 M. Karanik, D. Lesage, Y. Gimbert, P. Nava, S. Humbel, L. Giordano, G. Buono and J.-C. Tabet, *Organometallics*, 2011, **30**, 4814–4821.
40 A. W. Sromek, M. Rubina and V. Gevorgyan, *J. Am. Chem. Soc.*, 2005, **127**, 10500–10501.
41 F. Sabatelli, J. Segato, L. Belpassi, A. Del Zotto, D. Zuccaccia and P. Belanzoni, *Molecules*, 2021, **26**, 2445.